

Design and optimization of high-contrast gratings for multispectral VCSEL-SOI laser sources

I.S. Shashkin¹, M.I. Kondratov¹, A.E. Grishin¹, K.E. Pevchikh², S.O. Slipchenko¹, N.A. Pikhtin¹

¹Ioffe Institute, 194021, Russia, Saint-Petersburg, Politekhnikeskaya 26;

²Joint Stock Company "Zelenograd Nanotechnology Center",
124527, Russia, Moscow, Zelenograd, Solnechnaya alley 6, room IX, office 17

Abstract

In the scope of a computational experiment, high-contrast gratings (HCG) formed on a silicon-on-insulator (SOI) platform within vertical-cavity surface-emitting lasers (VCSELs) were studied for multispectral laser sources. A simulation model for spectral characteristics calculation is proposed, which includes two heterogeneously integrated parts of the VCSEL: 1) the lower output mirror based on a HCG grating in the silicon layer of the SOI surrounded by air cavities to enhance the contrast of the HCG; 2) the semiconductor VCSEL structure with an air aperture for current and optical confinement. Comparative analysis results of the spectral characteristics of VCSEL-SOI structures for zeroth, first, and second-order modes, which can be excited in the air aperture of the VCSEL, are presented. It is demonstrated that the HCG, acting as one of the cavity mirrors, effectively discriminates the VCSEL higher-order modes. An algorithm for calculating HCG parameters that ensure the maximum reflectivity at a fixed thickness of the silicon layer of the SOI is developed.

Keywords: high-contrast grating (HCG), HCG reflectivity for TE modes, vertical-cavity surface-emitting laser (VCSEL), silicon-on-insulator (SOI), heterogeneous integration.

Citation: Shashkin IS, Kondratov MI, Grishin AE, Pevchikh KE, Slipchenko SO, Pikhtin NA. Design and optimization of high-contrast gratings for multispectral VCSEL-SOI laser sources. *Computer Optics* 2024; 48 (4): 535-541. DOI: 10.18287/2412-6179-CO-1446.

Introduction

Vertical-cavity surface-emitting lasers (VCSELs) are compact laser sources with low heat dissipation, low threshold current and high efficiency (>60%). In the conventional design, the VCSEL chip is based on a planar heterostructure that determines the desired operating wavelength, while the lateral waveguide structure, formed through post-growth operations, determines the modal content of the output beam. At the same time, there are certain applications that require photonic integration where the emitters operate at specified wavelengths while maintaining single-mode operation. These applications include LiDAR systems for autonomous vehicles, optical transceivers for local area networks and data centers [1]. The challenge of creating the desired multispectral laser sources can be addressed by utilizing VCSEL designs implemented through heterogeneous integration techniques, where one of the VCSEL's cavity mirrors is formed within an SOI chip [2,3]. To use the SOI platform as a photonic waveguide, the VCSEL wavelength is selected within the range where silicon introduces minimal optical loss, specifically in the telecommunication wavelength range from 1260 nm (beginning of the O-band) to 1675 nm (end of the U-band).

The SOI platform provides the advantage of leveraging advanced silicon technology to fabricate complex planar photonic elements. The heterogeneous integration of A3B5 and SOI addresses the challenge of creating an efficient and readily available laser source

integrated with SOI-based photonic integrated circuits (PICs) [4]. Conversely, the use of external discrete semiconductor lasers within PICs has several drawbacks, including insertion loss, the need for individual precise adjustment, and increased overall dimensions [5]. In contrast, the VCSEL design within the heterogeneous integration approach comprises both a SOI part and an A3B5 heterostructure part [6]. The upper mirror of the VCSEL cavity, the emitting aperture, the lateral waveguide, and the active region are all fabricated within the A3B5 heterostructure part. It is worth noting that if the material gain spectrum of the A3B5 part does not cover the desired spectral range, modification of the active region in the A3B5 part will be necessary. In such cases, selective epitaxy technology is currently being developed to enable control over the characteristics of the grown layers in specific localized areas [7–9]. On the SOI substrate, the output mirror of the VCSEL cavity is fabricated, along with, if necessary, a layer specifically designed for outcoupling the light from the VCSEL cavity into the photonic waveguide of the PIC. The output mirror of the VCSEL cavity can be either a distributed Bragg reflector (DBR) [2] or a high-contrast grating (HCG) [3]. It is worth noting that compared to DBRs, HCGs offer higher reflectivity over a wider spectral range [10]. Another advantage of using HCG for forming the VCSEL cavity mirror is that HCG, unlike DBR, provides stable linear polarization of the VCSEL [11] and allows for discrimination of higher-order transverse modes by selecting the dimensions and positioning of the HCG

region with respect to the cavity axis [12]. To fabricate it, lithographic methods such as electron beam lithography, focused ion beam lithography, deep ultraviolet lithography, and nanoimprinting are used. It should be noted that for efficient operation of VCSEL with optimal laser characteristics, the power reflectivity of the VCSEL cavity output mirror needs to exceed 98% [13], which requires accurate optimization of the HCG parameters.

The first HCG-based mirror, which exhibits a wide reflection spectrum and high reflectivity, was proposed in [14]. The study emphasizes that, like any periodic structure, the HCG parameters scale with the wavelength. Furthermore, it provides an example of the HCG parameters scaling, at which the reflection spectrum is shifted from the 1.5 μm range to the 10 μm range without altering its characteristics. However, it is important to note that the HCG mirror reflectivity in the VCSEL-SOI heterogeneous structure depends on the divergence angle inside the cavity, which is determined by the VCSEL aperture parameters. As a result, the reflection spectrum of the HCG mirror in the VCSEL-SOI structure will change with variations in the wavelength, despite attempts to scale the HCG parameters. Additionally, it should be noted that experimentally fabricated gratings may have non-rectangular groove shapes [15, 16]. Consequently, employing advanced analytical approaches for HCG modeling that primarily describe the physical principles of its operation [17] becomes impractical. Therefore, there is a need for the development of numerical calculation algorithms that allow taking into account the features of experimental samples.

The present study of HCG spectral characteristics and its mode-selectivity properties in the VCSEL-SOI heterogeneous structure was carried out within a numerical experiment. We propose to use the SOI platform because it enables the fabrication of HCGs that cover various wavelength ranges and allows for the creation of multi-spectral laser sources through A3B5 bonding using a single SOI substrate. In the "Results and discussion" section, an optimization algorithm for HCG parameters is explored for several spectral ranges to create multi-spectral laser sources. Unlike prior research, our study introduces the simultaneous use of two approaches. Firstly, we propose surrounding the HCG with air regions to increase the refractive index contrast and achieve the maximum reflectivity of the HCG mirror for a given SOI silicon layer thickness. This approach aims to optimize the performance of the HCG structure. Secondly, we suggest selectively etching the SOI substrate along the output beam propagation path to ensure stable VCSEL operation without feedback from external elements or additional boundary interfaces. This technique enhances the overall performance of the device.

1. Simulation model

Fig. 1a illustrates the design of a single element of a multispectral source based on a heterogeneously integrat-

ed VCSEL-SOI structure. In the considered configuration, the emission is extracted from the structure through the lower HCG mirror, while the upper mirror is a DBR. The n-type InP layers serve as emitters and provide current spreading. The multiple quantum well (MQW) region may also include a tunnel junction, spacers, and waveguides. An example of the semiconductor part of the VCSEL structure is presented in [18]. The developed design is based on the following assumptions: (1) the transition to the SOI part is realized through an adhesive layer, which is negligibly thin, since previous studies [19] have demonstrated that the thickness of such a layer can be approximately $40 \text{ nm} \pm 5 \text{ nm}$; (2) a layer of SiO_2 , referred to as the top oxide (TOX), is present between the InP layer and SOI, and its thickness is one of the model parameters; (3) the SOI substrate has standard thicknesses from the dimensional series, with the silicon layer being 400 nm, and the layer of the bottom oxide (BOX) SiO_2 being 2000 nm; (4) to achieve optimal performance of the HCG, the region of the TOX layer between the InP layer and the silicon layer of the SOI substrate that lies along the path of the laser beam inside the VCSEL cavity is selectively etched; (5) the BOX layer and the silicon substrate beneath the silicon layer of the SOI are also selectively etched in the region along the path of the laser beam exiting the resonator. While these features, individually described in (4) and (5), have been proposed before, their combination here is a novel approach based on an extensive literature review and patent search. The selective wet etching technique [6] can be employed to remove the TOX and BOX layers, as well as the silicon layer of the SOI substrate. It is important to note that as a result, the HCG is surrounded by air cavities, which provide a high reflection coefficient due to the significantly high refractive index contrast.

Numerical calculations were conducted for the region delineated by the red dashed line in Fig. 1a. The study was based on the following assumptions: (1) the semiconductor region of the computational domain comprises the InP layer and the MQWs region with adjacent air regions for the lateral optical and current confinement, which defines the aperture inside the VCSEL cavity; (2) the SOI region of the computational domain encompasses the SOI area with the HCG and includes air regions resulting from the selective etching of TOX and BOX layers that are adjacent to the HCG and the etched substrate region.

The computational domain is constructed in Comsol using the "Electromagnetic Waves, Frequency Domain" interface of the "Wave Optics" module. Given that both the fundamental mode and higher-order modes can be excited at the VCSEL aperture, the calculation of the HCG mirror reflectivity involves an initial step of determining the effective refractive indices corresponding to the modes of interest using the "Boundary Mode Analysis" interface. In the subsequent step, the electromagnetic

field with TE polarization (the electric field vector E is parallel to the HCG grooves) is computed across the entire computational domain. This computation is performed for a selected mode profile at the aperture, corresponding to a chosen effective refractive index of the aperture mode. The reflectivity is subsequently calculated as the square modulus of the S_{11} parameter, based on the initial field distribution at the aperture, which corresponds to the mode profile obtained in the first step, and the resulting field distribution at the aperture obtained from the field computed for the entire computational domain.

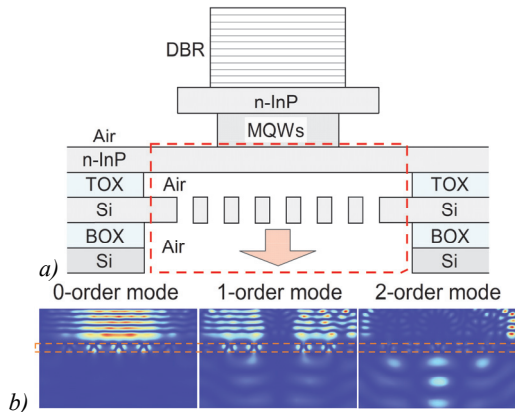


Fig. 1. (a) Schematic of a VCSEL-SOI structure with an HCG mirror. The red dashed line delineates the computational domain. The arrow indicates the direction of the output beam. (b) TE field distributions for cavity modes of 0th, 1st, and 2nd order upon reflection from the HCG optimized for maximum of 0th-order mode reflectivity at a wavelength of 1530 nm in the regions adjacent to the HCG. The orange dashed line marks the HCG domain

Based on the preliminary analysis, it has been determined that the HCG mirror reflectivity for modes of various orders, such as the 0-order mode, 1-order mode, and so on, becomes independent of the number of periods within the computational domain when the number of periods exceeds 9. Therefore, in the model, 12 periods are specified. The shape of the grating grooves is chosen to be rectangular. The refractive index of silicon is taken from [20] at a temperature of 293 K. The width of the air aperture and the refractive index of its central part (MQW region) are arbitrarily chosen as $6\ \mu\text{m}$ and 3.27, respectively. The thickness of the InP layer is 430 nm, and the refractive index of InP is taken from reference [21]. The width of the computational domain is $43\ \mu\text{m}$.

After determining the HCG parameters based on the proposed algorithm, the semiconductor part of the VCSEL-SOI structure needs to be optimized. This involves calculating the VCSEL-SOI cavity mode profile and determining the appropriate thicknesses of layers in the A3B5 part of the structure that ensure the following: (1) the lasing wavelength is matched to the reflection spectrum peak, (2) a high optical confinement factor in the active region, (3) the minimum optical confinement factor within the region of a tunnel p-n junction, (4) the DBR mirror reflectivity of 99.99% to minimize the threshold density. The device fabrication process involves

the following steps: (1) deposition of the TOX layer on the SOI substrate, (2) formation of air holes within the SOI-TOX structure, involving the creation of voids from both the substrate side and TOX side, extending all the way down to the silicon layer sandwiched between the TOX and BOX layers, (3) HCG formation in the silicon layer within the air holes, (4) deposition of an adhesion layer on the InP layer of the A3B5 part, (5) adhesive bonding between the A3B5 part and the SOI-TOX structure, (6) formation of the lateral waveguide structure, (7) formation of ohmic contacts (Fig. 1a).

2. Results and discussion

In this section, we describe the algorithm for searching optimal HCG parameters in the heterogeneously integrated VCSEL-SOI structure, ensuring maximum reflectivity. Below, we will present examples of optimizing HCG parameters for three wavelength ranges centered at 1300 nm, 1530 nm, and 1570 nm.

For each selected central wavelength and the fundamental mode excited at the aperture, the first stage of the optimization process is proposed to involve scanning the period and fill factor of the HCG. Parametric calculation results for the central wavelength of 1530 nm are shown in Fig. 2. The inset of Fig. 2 illustrates the reflectivity dependencies for all possible values of the fill factor for several HCG periods. It is evident that the maximum values lie approximately at a fill factor of 50%. Therefore, the boundaries of the search area for optimal parameters can be chosen close to this value to save overall search time. Additionally, Fig. 2 reveals that each curve corresponding to a specific HCG period has a maximum at a certain fill factor, and the position of the reflectivity maximum shifts towards lower period values as the fill factor increases. As a result, the HCG period and fill factor are determined that provide the maximum reflectivity. For the studied central wavelengths, the optimal period and fill factor values are given in Tab. 1.

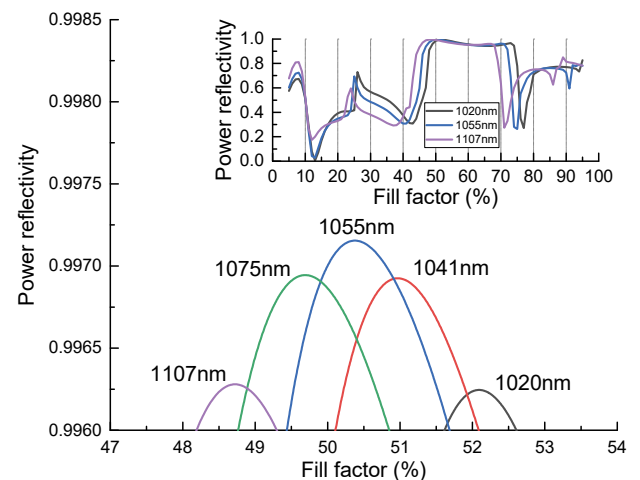


Fig. 2. Power reflectivity as a function of fill factor for several HCG periods. HCG period values are indicated, with a fixed HCG silicon layer thickness of 400 nm, TOX thickness of 400 nm, and a wavelength of 1530 nm

Tab. 1. Calculation results using the proposed algorithm for studied central wavelengths with a 400-nm-thick SOI silicon layer, an effective cavity length of 3.5 μm, and a DBR mirror reflectivity of 99.99 %.

Parameter name	Parameter value for a given central wavelength		
Central wavelength	1300 nm	1530 nm	1570 nm
HCG period	846 nm	1055 nm	1091 nm
HCG fill factor	48.75 %	50.4 %	50.4 %
TOX thickness	390 nm	360 nm	390 nm
0th order mode reflectivity	99.07 %	99.73 %	99.73 %
1st order mode reflectivity	97.47 % – R _{max} @1296 nm (not at 1300 nm: 96.89 %)	99.09 % – R _{max} @1521 nm (not at 1530 nm: 99.02 %)	99.02 % – R _{max} @1566 nm (not at 1570 nm: 99.00 %)
2nd order mode reflectivity	94.88 % – R _{max} @1291 nm (not at 1300 nm: 92.18 %)	98.2 % – R _{max} @1520 nm (not at 1530 nm: 97.96 %)	97.55 % – R _{max} @1523 nm (not at 1570 nm: 97.39 %)
0th order mode output loss	13.5 cm ⁻¹	4 cm ⁻¹	4 cm ⁻¹
1st order mode output loss	36.8 cm ⁻¹ – R _{max} @1296 nm: 97.47 % (not at 1300 nm: 96.89 %, 45.3 cm ⁻¹)	13.2 cm ⁻¹ – R _{max} @1521 nm: 99.09 % (not at 1530 nm: 99.02 %, 14.2 cm ⁻¹)	14.2 cm ⁻¹ – R _{max} @1566 nm: 99.02 % (not at 1570 nm: 99.00 %, 14.5 cm ⁻¹)
2nd order mode output loss	75.2 cm ⁻¹ – R _{max} @1291 nm: 94.88 % (not at 1300 nm: 92.18 %, 116.5 cm ⁻¹)	26.1 cm ⁻¹ – R _{max} @1520 nm: 98.2 % (not at 1530 nm: 97.96 %, 29.6 cm ⁻¹)	35.6 cm ⁻¹ – R _{max} @1523 nm: 97.55 % (not at 1570 nm: 97.39 %, 37.9 cm ⁻¹)

In the second stage of the algorithm, the thickness of the air gap between the HCG and InP layer is scanned using the optimal period and fill factor values calculated in the first stage (Fig. 3). The air gap thickness can be varied by selecting the TOX layer thickness, which is subsequently selectively removed before heterogeneous integration. As a result, the optimal TOX thickness is determined that provides the maximum reflectivity. The dependence of reflectivity on TOX thickness shows that the HCG reflectivity exhibits relatively low sensitivity to changes in TOX thickness. In the vicinity of the peak reflectivity obtained at the 1530 nm wavelength, the reflectivity will decrease by no more than 0.1 % to reach 99.63 % when varying the TOX thickness within ± 109 nm from the optimal value. Fig. 3 also demonstrates how wide the range of TOX thickness variation is, in which the reflection coefficient changes by only 0.1 %. The TOX thickness values optimal in terms of the maximum reflectivity for the selected wavelengths are given in Table 1. However, it should be noted that in systems where maximum modulation speed is required, the aim is to minimize the cavity thickness between the HCG and A3B5 structure, which is determined by the TOX layer thickness, in order to reduce the cavity mode volume [6].

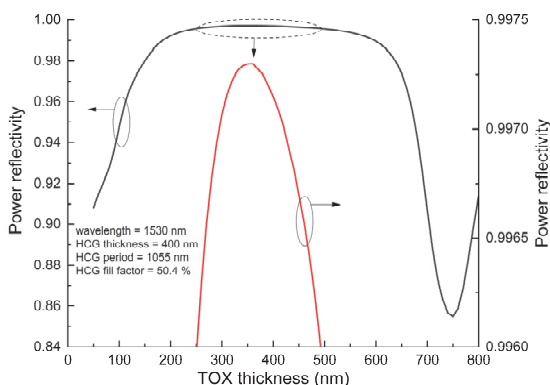


Fig. 3. Power reflectivity as a function of TOX thickness. The peak region is shown enlarged

The third stage of the proposed algorithm involves the calculation of reflectivity spectra for the 0th, 1st, and 2nd order modes using the optimal period, fill factor, and TOX thickness values obtained in the first and second stages. As an example, Fig. 4 shows the reflection spectra computed for modes of the indicated orders in the range, centered at a wavelength of 1530 nm. The spectral dependences of the reflectivity for the 0th, 1st and 2nd order modes exhibit noticeable differences. Specifically, throughout the entire spectral range, the reflectivity for the 0th order mode is higher than that of the higher order modes. Fig. 1b displays TE field distributions in the regions adjacent to the HCG for the cavity modes of orders 0, 1, and 2 as they reflect off the HCG, which parameters have been optimized to deliver maximum reflectivity for the 0th-order mode at a wavelength of 1530 nm. The asymmetry in the TE field distribution is a result of the computational domain's asymmetry, which does not impact the calculated reflectivities. Furthermore, it is worth noting that there is a shift in the reflectivity spectrum peak towards shorter wavelengths as the mode order increases relative to the central wavelength within the calculated range. To analyze the contribution of the obtained superiority of the 0th order mode reflectivity over the reflectivity of the higher order modes in discriminating against them, a calculation was conducted. This calculation allowed us to determine the extent to which the output losses for the higher order modes would exceed those for the 0th order mode. The output losses that contribute to the lasing threshold condition can be calculated using the relation $-0.5 \cdot \ln(R_1 \cdot R_2) / L$, where R_1 and R_2 are the power reflectivities of the mirrors, and L is the cavity length. For an effective cavity length of 3.5 μm, the output losses will increase by approximately 15 cm⁻¹ for every 1 % decrease in the HCG reflectivity. This relationship holds true when the power reflectivity of the output mirror for the 0th mode is above 98 % and for higher order modes is above 88 %. At 1530 nm, the

power reflectivities of the higher order modes are lower by 0.7% for the 1st order mode and 1.8% for the 2nd order mode compared to the 0th mode. This difference in power reflectivity corresponds to the 0th order mode having an advantage in the output loss gap of approximately 10 cm^{-1} and 26 cm^{-1} compared to the 1st and 2nd order modes, respectively. The calculated reflectivities and output losses are presented in Table 1. Based on the results, it can be presupposed that if the internal optical loss does not depend on the mode order, lasing of only the fundamental mode will be ensured.

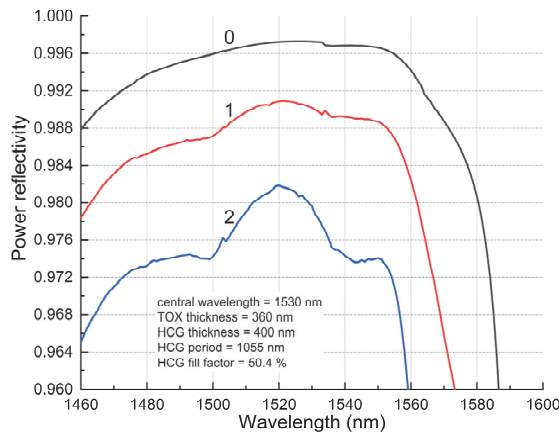


Fig. 4. HCG reflection spectra for 0th, 1st and 2nd order modes. The mode order is indicated by the number

Thus, the presented example demonstrates the algorithm for identifying the optimal HCG parameters in a heterogeneously integrated VCSEL-SOI structure. At each iteration, the algorithm identifies the optimal parameters that maximize the reflectivity. These optimal parameters are then used in the subsequent iterations, ensuring that the reflectivity is continually optimized throughout the process.

Fig. 5 shows reflection spectra for an HCG with a constant thickness of 400 nm. The spectra are calculated for three spectral ranges centered at 1300 nm, 1530 nm, and 1570 nm. These calculations were performed using the optimal values of HCG period, fill factor, and TOX thickness determined within the three stages of the algorithm.

It should be noted that the chosen silicon layer thickness in which the HCG is formed determines the width and peak of the reflection spectrum. The selected value of 400 nm is close to the optimum thickness for the $1.55 \mu\text{m}$ range.

Conclusion

As noted in the introduction section, the HCG parameters scale with wavelength. To maintain the width of the reflection spectrum and achieve the maximum reflectivity when transitioning from 1530 nm to 1300 nm, it is necessary to not only reduce the HCG period but also adjust the HCG layer thickness. This adjustment can be accomplished by selectively etching the silicon layer on the SOI substrate to achieve the desired thickness, particularly in the case of fabricating multi-wavelength laser sources on

a single SOI wafer. Alternatively, if only a single wavelength is required, selecting an SOI substrate with a smaller silicon layer thickness can be a suitable option. Thus, adjusting the silicon layer thickness offers flexibility in this regard.

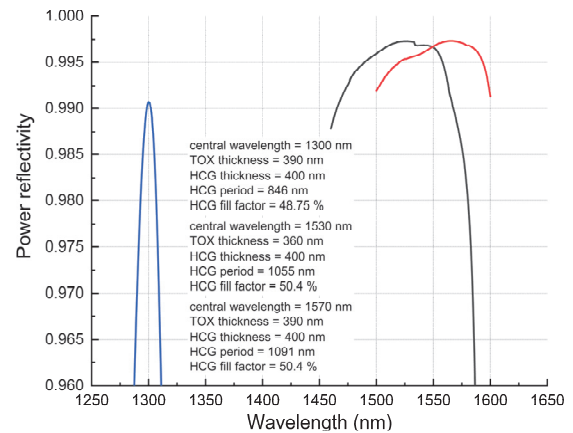


Fig. 5. Comparison of HCG reflection spectra for a grating with constant thickness of 400 nm. The reflectivity is calculated across three different spectral ranges centered at 1300 nm, 1530 nm, and 1570 nm. The indicated optimal values of the HCG period, fill factor, and top oxide (TOX) thickness determined from the proposed three-stage optimization algorithm were used in the calculations

However, an alternative option is also available, where the silicon layer thickness remains unchanged. It is worth noting the narrowness of the spectral line centered at a wavelength of 1300 nm, which exhibits a power reflectivity peak above 99%. This observation suggests the potential for spectral selectivity in a laser source operating in close proximity to this particular wavelength. The results shown in Figure 5 also demonstrate the potential for utilizing optimized HCG not only for spectral selection but also for spectrum stabilization, which can be achieved through a narrower HCG reflection spectrum.

In summary, a novel approach for multispectral VCSEL-SOI laser sources using optimized high-contrast gratings is proposed. The gratings are surrounded by air to maximize reflectivity. Emission through an air gap in SOI enables stable lasing. An algorithm optimizes grating parameters for high reflectivity. Effective discrimination of higher-order modes is demonstrated. The approach can enhance efficiency and performance of heterogeneous VCSEL-SOI lasers.

References

- [1] Babichev A, Blokhin S, Kolodeznyi E, Karachinsky L, Novikov I, Egorov A, Tian S-C, Bimberg D. Long-wavelength VCSELs: Status and prospects. *Photonics* 2023; 10(3): 268. DOI: 10.3390/photronics10030268.
- [2] Kumari S, Haglund EP, Gustavsson JS, Larsson A, Roelkens G, Baets RG. Vertical-cavity silicon-integrated laser with in-plane waveguide emission at 850 nm. *Laser Photon Rev* 2018; 12(2): 1700206. DOI: 10.1002/lpor.201700206.
- [3] Park GC, Xue W, Taghizadeh A, Semenova E, Yvind K, Mørk J, Chung I. Hybrid vertical-cavity laser with lateral

- emission into a silicon waveguide. *Laser Photon Rev* 2015; 9(3): L11-L15. DOI: 10.1002/lpor.201400418.
- [4] Roelkens G, Liu L, Liang D, Jones R, Fang A, Koch B, Bowers J. III-V/silicon photonics for on-chip and intra-chip optical interconnects. *Laser Photon Rev* 2010; 4(6): 751-779. DOI: 10.1002/lpor.200900033.
- [5] Lu H, Lee JS, Zhao Y, Scarcella C, Cardile P, Daly A, Ortsiefer M, Carroll L, O'Brien P. Flip-chip integration of tilted VCSELs onto a silicon photonic integrated circuit. *Opt Express* 2016; 24(15): 16258-16266. DOI: 10.1364/OE.24.016258.
- [6] Park GC, Xue W, Piels M, Zibar D, Mørk J, Semenova E, Chung I-S. Ultrahigh-speed Si-integrated on-chip laser with tailored dynamic characteristics. *Sci Rep* 2016; 6: 38801. DOI: 10.1038/srep38801.
- [7] Shamakhov V, Slipchenko S, Nikolaev D, Smirnov A, Eliseyev I, Grishin A, Kondratov M, Shashkin I, Pikhtin N. Selective area epitaxy of highly strained InGaAs quantum wells (980–990 nm) in ultrawide windows using metalorganic chemical vapor deposition. *Nanomaterials* 2023; 13(17): 2386. DOI: 10.3390/nano13172386.
- [8] Zhao X, McKenzie AF, Munro CW, Hill KJ, Kim D, Bayliss SL, Gerrard ND, MacLaren DA, Hogg RA. Large-area 2D selective area growth for photonic crystal surface emitting lasers. *J Cryst Growth* 2023; 603: 127036. DOI: 10.1016/j.jcrysgro.2022.127036.
- [9] Besancon C, Néel D, Make D, Ramirez JM, Cerulo G, Vaissiere N, Bitauld D, Pommereau F, Fournel F, Dupré C, Mehdi H, Bassani F, Decobert J. AlGaInAs multi-quantum well lasers on silicon-on-insulator photonic integrated circuits based on InP-seed-bonding and epitaxial regrowth. *Appl Sci* 2021; 12(1): 263. DOI: 10.3390/app12010263.
- [10] Chang-Hasnain CJ. High-contrast grating VCSELs. In Book: Michalzik R, ed. VCSELs. Fundamentals, technology and applications of vertical-cavity surface-emitting lasers. Berlin, Heidelberg: Springer; 2013: 291-317. DOI: 10.1007/978-3-642-24986-0_9.
- [11] Haglund A, Gustavsson JS, Bengtsson J, Jedrasik P, Larsson A. Design and evaluation of fundamental-mode and polarization-stabilized VCSELs with a subwavelength surface grating. *IEEE J Quantum Electron* 2006; 42(3): 231-240. DOI: 10.1109/JQE.2005.863703.
- [12] Gustavsson JS, Haglund Å, Vukusić JA, Bengtsson J, Jedrasik P, Larsson A. Efficient and individually controllable mechanisms for mode and polarization selection in VCSELs, based on a common, localized, sub-wavelength surface grating. *Opt Express* 2005; 13(17): 6626-6634. DOI: 10.1364/OPEX.13.006626.
- [13] Coldren LA, Corzine SW, Mašanović ML. Diode lasers and photonic integrated circuits. Hoboken, NJ: John Wiley and Sons Inc; 2012. DOI: 10.1002/9781118148167.
- [14] Mateus CFR, Huang MCY, Deng Y, Neureuther AR, Chang-Hasnain CJ. Ultrabroadband mirror using low-index cladded subwavelength grating. *IEEE Photonics Technol Lett* 2004; 16(2): 518-520. DOI: 10.1109/LPT.2003.821258.
- [15] Ferrara J, Yang W, Zhu L, Qiao P, Chang-Hasnain CJ. Heterogeneously integrated long-wavelength VCSEL using silicon high contrast grating on an SOI substrate. *Opt Express* 2015; 23(3): 2512-2523. DOI: 10.1364/oe.23.002512.
- [16] Ferrara J, Zhu L, Yang W, Qiao P, Chang-Hasnain CJ. Heterogeneously-integrated VCSEL using high-contrast grating on silicon. *Proc SPIE* 2015; 9372: 937208. DOI: 10.1117/12.2079732.
- [17] Karagodsky V, Chang-Hasnain CJ. Physics of near-wavelength high contrast gratings. *Opt Express* 2012; 20(10): 10888-10895. DOI: 10.1364/OE.20.010888.
- [18] Park M-R, Kwon O-K, Han W-S, Lee K-H, Park S-J, Yoo B-S. All-monolithic 1.55 μm InAlGaAs/InP vertical cavity surface emitting lasers grown by metal organic chemical vapor deposition. *Jpn J Appl Phys* 2006; 45(11): L8. DOI: 10.1143/JJAP.45.L8.
- [19] Haglund EP, Kumari S, Westbergh P, Gustavsson JS, Roelkens G, Baets R, Larsson A. Silicon-integrated short-wavelength hybrid-cavity VCSEL. *Opt Express* 2015; 23(26): 33634-33640. DOI: 10.1364/OE.23.033634.
- [20] Li HH. Refractive index of silicon and germanium and its wavelength and temperature derivatives. *J Phys Chem Ref Data* 1980; 9(3): 561-658. DOI: 10.1063/1.555624.
- [21] Adachi S. Optical dispersion relations for GaP, GaAs, GaSb, InP, InAs, InSb, $\text{Al}_x\text{Ga}_{1-x}\text{As}$, and $\text{In}_{1-x}\text{Ga}_x\text{As}_y\text{P}_{1-y}$. *J Appl Phys* 1989; 66(12): 6030-6040. DOI: 10.1063/1.343580.

Authors' information

Ilya Sergeevich Shashkin, born in 1986 in Leningrad, received the M.S. degree in Engineering of Laser Systems from the Baltic State Technical University «VOENMEH» named after D.F. Ustinov in 2009, and the Ph.D. degree in Semiconductor Physics from the Ioffe Institute in 2012. Currently, he is a member of the staff at the Centre of Nanoheterostructure Physics, Ioffe Institute, Saint-Petersburg, Russia. His research is primarily on the physics associated with semiconductor lasers. E-mail: shashkin@mail.ioffe.ru <https://orcid.org/0000-0002-8583-2935>

Matvey Igorevich Kondratov, postgraduate student. He is a member of the staff at the Centre of Nanoheterostructure Physics, Ioffe Institute, Saint-Petersburg, Russia. His area of scientific interest focuses on the development of injection lasers based on A3B5 semiconductor heterostructures. E-mail: mikondratov@mail.ioffe.ru

Artyom Evgenyevich Grishin, postgraduate student. He is a member of the staff at the Centre of Nanoheterostructure Physics, Ioffe Institute, Saint-Petersburg, Russia. His area of scientific interest focuses on the development of injection lasers based on A3B5 semiconductor heterostructures. E-mail: ar.grish@mail.ioffe.ru

Konstantin Eduardovich Pevchikh, Advisor to the General Director at Joint Stock Company “Zelenograd Nanotechnology Center”. He is actively engaged in the development of optical sensors based on silicon-on-insulator structures. E-mail: pevchikh@gmail.com <https://orcid.org/0009-0009-5629-6262>

Sergey Olegovich Slipchenko, Ph.D. He is a member of the staff at the Centre of Nanoheterostructure Physics, Ioffe Institute, Saint-Petersburg, Russia. His area of scientific interest focuses on the development of injection lasers based on A3B5 semiconductor heterostructures. E-mail: serghpl@mail.ioffe.ru <https://orcid.org/0000-0003-4851-3641>

Nikita Aleksandrovich Pikhtin, born in 1966 in Leningrad, received the Ph.D. in 2000. Presently he is the acting head of Semiconductor Luminescence and Injection Emitters Laboratory and the head of the Centre of Nanoheterostructure Physics at Ioffe Institute, Saint-Petersburg, Russia. He is dealing with the design, development and fabrication of high power laser diodes and devices on their base emitting in 650-1800 nm wavelength range. He is an author of more than 200 papers in national and international journals and Conference Proceedings. E-mail: nike@hpld.ioffe.ru <https://orcid.org/0000-0002-0492-2227>

Code of State Categories Scientific and Technical Information (in Russian – GRNTI): 29.33.39, 29.19.31, 29.33.15, 29.33.43

Received October 27, 2023. The final version – January 15, 2024.
